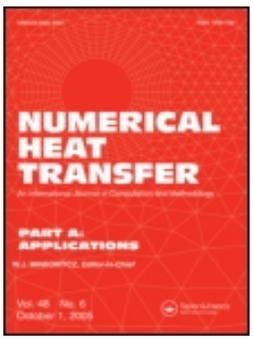

Numerical Heat Transfer, Part A: Applications

ISSN: 1040-7782 (Print) 1521-0634 (Online) Journal homepage: http://www.tandfonline.com/loi/unht20

Application of the Conservative Discrete Transfer Radiation Method to a Furnace with Complex Geometry

Mario Baburić , Neven Duić , Alexandre Raulot & Pedro J. Coelho

To cite this article: Mario Baburić , Neven Duić , Alexandre Raulot & Pedro J. Coelho (2005) Application of the Conservative Discrete Transfer Radiation Method to a Furnace with Complex Geometry, Numerical Heat Transfer, Part A: Applications, 48:4, 297-313, DOI: 10.1080/10407780590945498

To link to this article: http://dx.doi.org/10.1080/10407780590945498

Published online: 02 Sep 2006.

Numerical Heat Transfer, Part A, 48: 297–313, 2005

ISSN: 1040-7782 print/1521-0634 online
DOI: 10.1080/10407780590945498

Taylor & Francis
Taylor & Francis Group

APPLICATION OF THE CONSERVATIVE DISCRETE TRANSFER RADIATION METHOD TO A FURNACE WITH COMPLEX GEOMETRY

Mario Baburić and Neven Duić
Faculty of Mechanical Engineering and Naval Architecture, University of Zagreb, Zagreb, Croatia

Alexandre Raulot
AVL France S.A., Espace Claude Monet, Croissy-sur-Seine, Paris, France

Pedro J. Coelho
Instituto Superior Técnico, Mechanical Engineering Department, Lisboa, Portugal

A conservative form of the discrete transfer radiation method (DTRM) has been applied in a computational fluid dynamics (CFD) simulation of the radiative heat transfer in an experimental furnace with complex geometry. The furnace was operated under nonpremixed conditions, burning preheated heavy fuel oil. For combustion simulation a semiempiric oil combustion model has been applied, while for the flow field resolution an unstructured CFD code has been used. The simulation results are compared with available experimental data, showing acceptable level of prediction accuracy. The conservative DTRM formulation is shown to be superior to the original formulation in this particular case.

INTRODUCTION

A computational fluid dynamics (CFD) simulation of the physical processes in an experimental furnace with complex geometry has been performed. The Furnace Trial M-1 at the Research Station of the International Flame Research Foundation at IJmuiden (Netherlands) was selected, and the experimental data from Johnson's Ph.D. thesis [1] were used for validation purposes. The complete mathematical description of physical processes in a furnace requires appropriate modeling of various phenomena, such as combustion, turbulent flow, convection and radiation heat transfer, etc., which, together with numerical techniques employed for their solution, results in a complex and demanding solution procedure. This work is focused particularly on radiative heat transfer simulation in such a complex case. The importance

Received 15 October 2004; accepted 30 December 2004.
A preliminary version of this article was presented at CHT-04: An ICHMT International Symposium on Advances in Computational Heat Transfer, April 2004, G. de Vahl Davis and E. Leonardi (eds.), CD-ROM Proceedings, ISBN 1-5670-174-2, Begell House, New York, 2004.
Address correspondence to Mario Baburić, Faculty of Mechanical Engineering and Naval Architecture, University of Zagreb, I. Lučića 5, 10000 Zagreb, Croatia. E-mail: Mario.Baburic@fsb.hr

NOMENCLATURE

A	area	in	incoming
C_R	correction factor	j	point-face index
I	radiant intensity	k_j	source contribution in intersected control volume of a ray around face j (which intersects it)
$\vec{n}$	normal vector		
N	total number		
q	total radiant power per unit area	n	position where a ray enters into the nth control volume
$\vec{s}$	rays direction vector		
$\overline{S}$	energy source due to radiation	$n+1$	position where a ray leaves the nth control volume
T	temperature		
ε	total emissivity	out	outgoing
Θ	polar angle	rays	rays
σ	Stefan-Boltzmann constant	tot	total (number)
Ω	solid angle	w	wall
		0	beginning of incremental path
Subscripts			
i	direction		

of radiative heat transfer in overall heat balance of such large-scale furnaces has been emphasised by many researchers. The importance of accurate heat transfer modeling in various devices of practical interest, e.g., gas turbines, boilers, furnaces, etc., and its impact on pollutant formation, are sufficient reasons to stay focused on searching for good radiation solutions.

The application of CFD techniques, while solving various problems of engineering interest, has been widespread among researchers in the last two decades. Some sort of general formulation has been established already, and modeling of many different physical phenomena, such as turbulence, combustion, multiphase flow, etc., fits well into this solution procedure. However, the inclusion of radiation modeling into this common framework is not that straightforward, and many different approaches have been used to account for it. Some early methods, such as Hottel's zone method [2] or the Monte Carlo technique applied to radiative heat transfer problems [3], although accurate, have not found wide usage, mostly due to their poor computational economy. Three methods of choice, when radiation prediction in various combustion systems is attempted, and which are sufficiently economical, are the discrete ordinates method [4, 5], the finite-volume method [6], and the discrete transfer method [7]. Due to sufficient generality and their conformance with control-volume formulations, their implementations can be found in some major CFD codes nowadays.

The validation of various radiation methods in the past has been performed mainly by simulating some standard test cases with simple geometries [8], where under certain presumptions the exact analytical solutions could be obtained, making these cases appropriate for evaluation of radiation models. However, in practical situations, problems with simple geometries are rather seldom found, and assessment of radiation models in problems with complex geometries seems to be necessary. Not many studies on radiation model assessment on complex geometry have been reported in the past. Adams and Smith [9] reported a 3-D simulation of a furnace with complex geometry, with a configuration very similar to that used in this work,

emphasizing the importance of intrusions (water tubes, superheater panels, etc.) modeling when overall heat fluxes are concerned. They focused on radiation itself (discrete ordinates method), taking all other necessary parameters, such as velocities, temperatures, radiative properties (emissivities), etc., from the available experimental data. Kim et al. [10] applied the finite-volume radiation method to the same configuration as well.

In the present work, a complete CFD simulation has been performed, including resolution of the turbulent flow field, combustion, radiation, etc. The program applied for the calculations was AVL's unstructured CFD code SWIFT [11]. After the standard discrete transfer radiation method (DTRM) was implemented into SWIFT code and validated on simple test cases [12, 13], the IJmuiden Furnace Trial M-1 [1] example seemed appropriate for further assessment of the implementation and the method itself. Coelho et al. [14] demonstrated in their work some drawbacks of the standard DTRM formulation, emphasizing the inherent problem of this formulation when overall energy conservation is considered. A new conservative formulation of the discrete transfer method is proposed there and it has been implemented into SWIFT and applied in this work subsequently. The simulation results were compared with the available experimental data, with the primary objective being evaluation of the heat fluxes at the side walls and cooling tubes. A simple sensitivity analysis on different number of rays used in DTRM simulation has been done as well.

A short theoretical description of the mathematical model is given below, while the experimental and computational details are presented subsequently. Afterwards, the simulation results are presented and compared with available experimental data. Finally, some conclusions are drawn.

MATHEMATICAL MODELING OVERVIEW

The solution procedure applied in this work is based on appropriate mathematical models coupled to an unstructured steady-state fluid flow solver, as available in SWIFT code [11]. The unstructured computational mesh was generated by the automatic mesh generator FAME HYBRID [15]. The mesh had 836,951 control volumes, with approximately 75% of them being hexahedrals. Adams and Smith [9] showed that simulation results in a similar case are pretty insensitive to mesh size, with more dense resolution being the only benefit of using a finer mesh. The turbulent flow field was resolved by using the standard k–ε model. Its robustness and relatively low computational demands were the decisive reasons for this choice. Due to swirl motion present in the current case, more advanced turbulence modeling, such as second-moment closure models, would probably yield a better flow pattern, but it was not used here due to limited computational power being available. A semiempiric oil combustion model [16] has been employed for combustion simulation. It is based on a single-step irreversible reaction scheme, with functionally prescribed mean reaction rate in an Arrhenius-type expression. The advantage of this model lies in the fact that costly spray calculations could be avoided, with droplet heat induction and evaporation times being empirically prescribed within the reaction rate definition. This combustion model is rather simple, but its robustness and simplicity

were the decisive reasons to apply it here, whereas for detailed simulation of combustion much more computational power would be necessary. The radiative properties of participating media were evaluated according to the weighted sum of gray gases model (WSGGM) and polynomial coefficients of Smith et al. [17]. In this model carbon dioxide (CO_2) and water vapor (H_2O) are the only gaseous species participating in overall radiation heat exchange.

CONSERVATIVE DISCRETE TRANSFER RADIATION METHOD

The discrete transfer radiation method presumes that radiation intensity through a solid angle can be approximated by a single ray. The method consists of tracking the intensity changes for a specified number of rays that are fired from a radiant surface (boundary) cell face, covering the hemisphere above it (see Figure 1).

The following formula is used to track the changes in radiant intensity along the ray:

$$I_{n+1} = I_n(1 - \varepsilon) + \varepsilon \frac{\sigma T^4}{\pi} \tag{1}$$

In this equation, I stands for radiant intensity and indices n and $n + 1$ specify the locations where a ray enters and leaves the control volume on which the equation is applied, respectively (Figure 2). The symbol ε represents the total emissivity and is modeled according to the WSGGM [17]. The symbol σ is the Stefan-Boltzmann constant, while T is the temperature in the control volume under consideration.

Within the CFD framework, the solution procedure for radiative transfer consists of performing the ray-tracing calculations first. In this part, the rays are fired from all boundary faces that participate in radiant exchange and each ray is tracked,

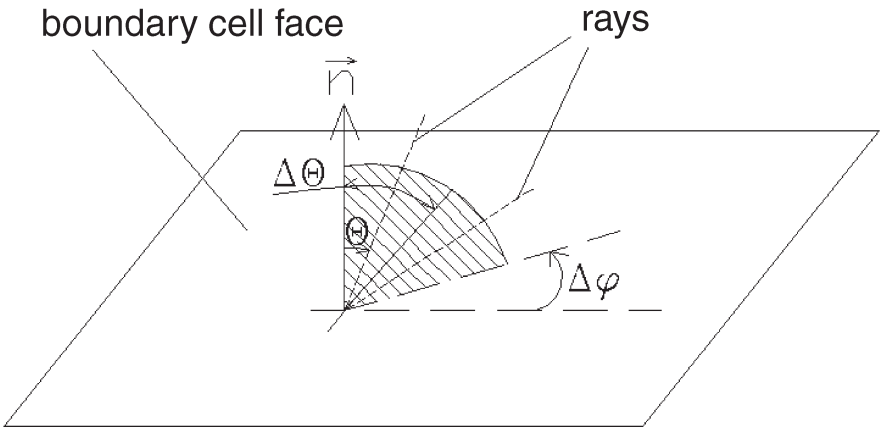

Figure 1. Hemisphere discretization around a boundary cell face (cut).

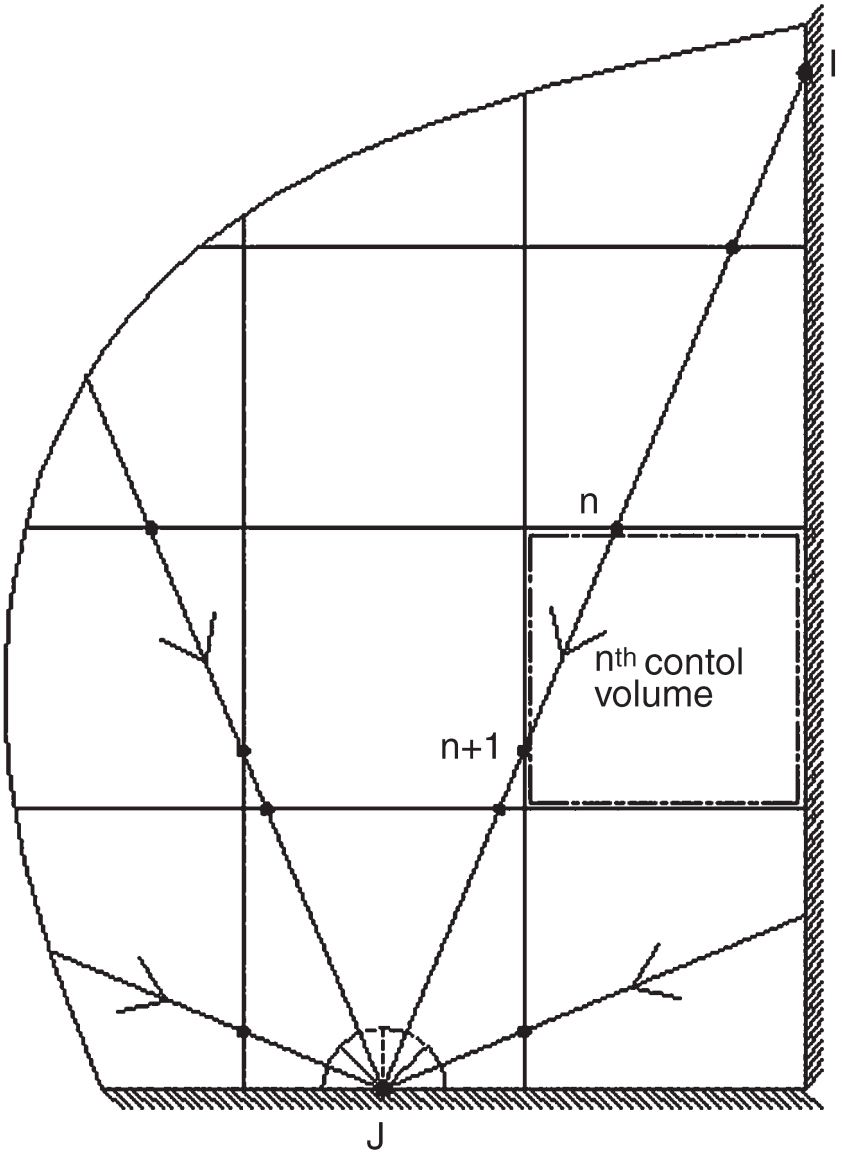

Figure 2. Ray around boundary cell face J (2-D projection).

together with its intersection with control volumes that it passes through, until an opposite boundary is reached. This part is done only once and in a preprocessor step, and all geometric information is saved into a file. When all ray paths are known, as well as their intersections with control volumes, the radiation exchange can be calculated by using Eq. (1).

In order to start the calculation from the opposite boundary according to Eq. (1), the value of leaving radiant intensity I_0 is needed. This value is obtained

from appropriate boundary treatment. It is customary to assume that radiant surfaces are gray and obey the Lambert cosine law, leading to the following boundary relation:

$$I_0 = \frac{q_{\text{out}}}{\pi} = \frac{q_{\text{in}}}{\pi}(1 - \varepsilon_w) + \varepsilon_w \frac{\sigma T_w^4}{\pi} \tag{2}$$

According to Eq. (2), the total radiant intensity leaving a boundary face consists of a reflected part (first term on the right-hand side) and a directly emitted part (second term on the right-hand side). In this equation, q_{in} represents the total radiant power per unit area that impinges the boundary face, while ε_w stands for the wall emissivity of the same face. T_w represents the cell face temperature.

The total hemispherical irradiation on a boundary cell face is obtained by collecting the incoming radiant intensities for all the rays fired from that face according to

$$q_{\text{in}} = \int_{\vec{s}\cdot\vec{n}<0} \overrightarrow{Is} \cdot \vec{n}\, d\Omega \approx \sum_{i=1}^{N_{\text{rays}}} I_i \cos\Theta_i \, \Delta\Omega_i \tag{3}$$

In Eq. (3), Θ_i is the angle between the ray direction vector and the boundary-face normal vector, while $\Delta\Omega_i$ represents the solid angle around the ray under consideration.

As each ray propagates through the domain, its radiative energy changes due to radiation of the participating medium, yielding a contribution to the source term of the energy equation. For a control volume that is intersected by a ray, the energy source due to radiant intensity change along this ray is calculated as

$$\overline{S}_{k_j} = (I_{n+1} - I_n) A_j \cos\Theta_j \, \Delta\Omega_j \tag{4}$$

A_j is the area of the boundary face from which the ray is emitted. The total energy source within a control volume is obtained by collecting the source terms due to all rays that intersect that control volume, i.e.,

$$\overline{S}_{\text{tot}} = \sum \overline{S}_{k_j} \tag{5}$$

In [14] it was noticed that the standard DTRM, as described by Eqs. (1)–(5), does not satisfy the conservation of energy exactly. Starting from this observation, it is then easy to find that, when thermal radiation is the only heat transfer mechanism, the overall net radiative flux at the boundary is not equal to the radiative power generated within the enclosure, i.e.,

$$\sum_{\text{faces\_}j} A_j \cdot (q_{\text{in}} - q_{\text{out}}) \neq \sum_{\substack{\text{internal} \\ \text{cells\_}i}} \overline{S}_i \tag{6}$$

As a result, a conservative formulation of the DTRM was proposed in [14]. A conservation correction factor C_R is defined as

$$C_R = \frac{\sum_{\text{faces\_}j} A_j \cdot q_{\text{out},j}}{\sum_{\substack{\text{starting} \\ \text{points\_}j}} \left[q_{\text{out},j} \cdot \left(\sum_{\substack{i=\text{ending\_points} \\ \text{of\_ray\_}j}} \cos\Theta_{i,j}\, \Delta\Omega_{i,j} A_i / \pi \right) \right]} \tag{7}$$

Then the intensity leaving the boundary face, which is calculated according to Eq. (2) in the standard procedure, is corrected as

$$I_0 = C_R \cdot \frac{q_{\text{out}}}{\pi} \tag{8}$$

Apart from that, the standard DTRM algorithm remains the same.

EXPERIMENTAL SETUP

Experimental work was carried out at the Research Station of the International Flame Research Foundation (IFRF) at IJmuiden, the Netherlands, as a part of the Furnace Trial M-1 [1]. The furnace is constituted of a horizontal tunnel constructed of refractory brickwork (450 mm), approximately square in cross section (2 m × 2 m), with an arched roof, and a length of 6.25 m. The general furnace layout is shown in Figure 3.

The fuel and air streams are injected through a replaceable burner system in one end wall, the usual arrangement being for a single horizontal flame fired axially along the length of the furnace and exhausting through a chimney at the far end of the furnace. The burner is carried within a removable water-cooled surround so that different flames can be studied simply by changing the burner configuration. Air is

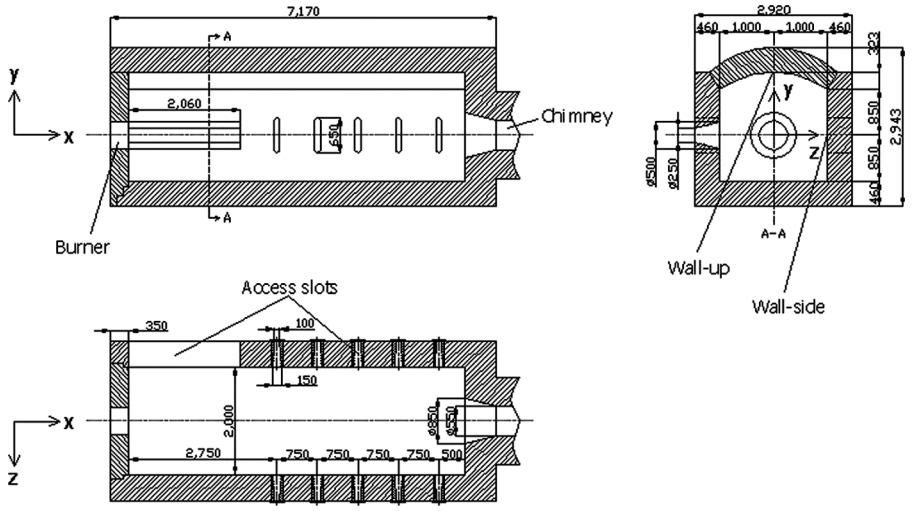

Figure 3. Furnace no. 1 (Furnace Trial M-1, [1]) general layout.

supplied in two streams, primary and secondary, and each one can be controlled and preheated separately. The fuel supplied can be oil, gas, or pulverized coal. In our case it is preheated oil. Access to the flame for measurement purposes is provided by a number of slots through the furnace walls. The heat input to the furnace can be varied over a wide range, but the usual heat input rate is about 1,500–1,800 kW. Heat is removed from the furnace by chimney losses, conduction through the furnace walls, and water cooling to the access doors, the burner surround, and cooling tubes.

The heat removed from the furnace by means of the water-cooled access doors, the burner surround, and the special double-loop-arranged cooling tubes, was measured during the trial. The basic principle used was to measure the water flow rate and the temperature rise of the water through the system. The cooling-tubes arrangement and their positioning can be seen in Figure 4.

The burner was required to give a simple overall furnace aerodynamic pattern, with a relatively long flame, a short ignition distance, and good stability. Figure 5 shows a general arrangement of the burner. The central fuel injector terminates in a pressure jet oil atomizer. The fuel is injected into a precombustion chamber formed by a divergent nozzle followed by a cylindrical extension of variable length. A part of the combustion air (the primary air) is supplied around the fuel injector through the divergent nozzle, the remaining air (secondary air) being supplied through a concentric annular nozzle outside the precombustion chamber. The primary air enters the precombustion chamber through a small swirler, in order to establish a central reverse-flow region inside the burner quarl and thus stabilize ignition near the nozzle throat. The secondary air is not swirled.

In Trial M-1, oil fuel with the following characteristics has been used:

Oil: 800 sec. Fuel oil	
Composition (mass fractions):	
Carbon	0.869
Hydrogen	0.118
Sulfur	0.010
Lower calorific value	41,000 kJ/kg
Viscosity at 110°C	14.1×10^{-6} m^2/s

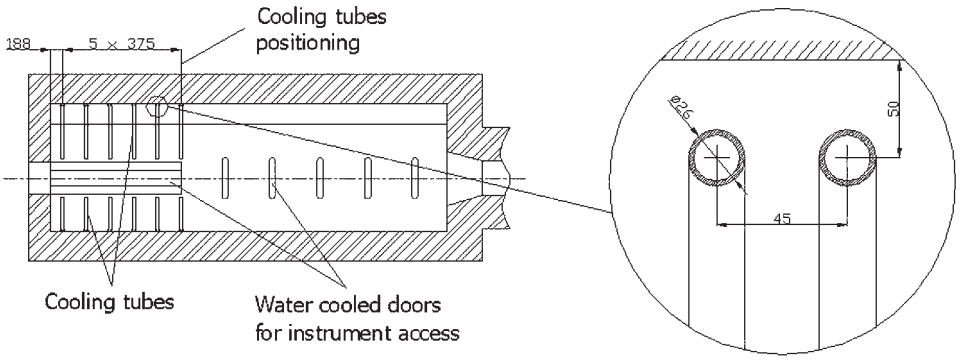

Figure 4. Cooling-tubes arrangement.

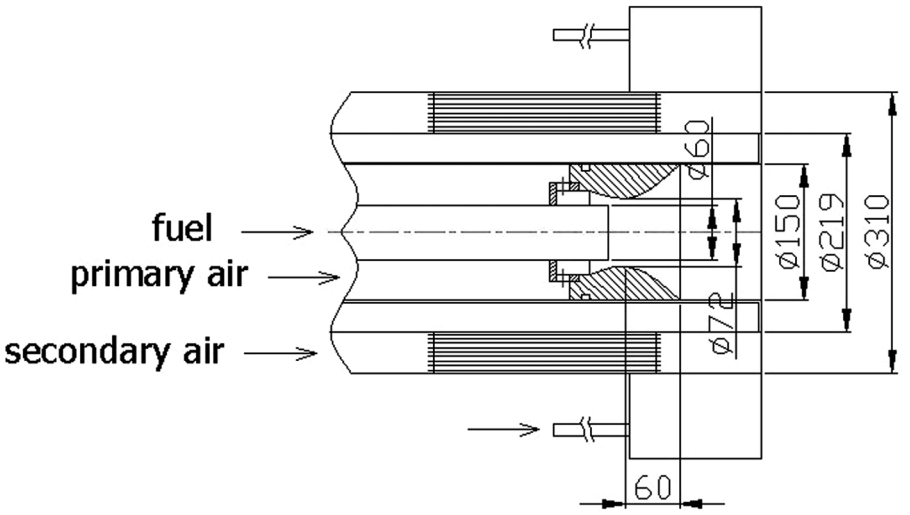

Figure 5. Burner arrangement.

The input parameters at the fuel and air inlets, resulting in a total heat input of 1,806 kW, were

Secondary air mass flow	1,849 kg/h
Primary air mass flow	434 kg/h
Fuel mass flow	155 kg/h
Secondary air temperature	47°C
Primary air temperature	26°C
Fuel temperature	116°C

For more details on the experimental setup, refer to [1].

COMPUTATIONAL DETAILS

According to the experimental arrangement described above, the computational grid has been generated using the FAME HYBRID [15] mesh generator. The modeling of cooling tubes, which are relatively small when compared to the rest of the domain, resulted in an increased number of computational cells (control volumes; total 836,951) that had to be used in order to capture all the geometric details. Figure 6 shows a vertical cut through part of the mesh and along the axis, where dense cell distribution can be observed in the vicinity of cooling tubes and around the burner region. The mesh has been additionally refined around the axis, in the flame-expecting region. The mesh was unstructured.

At the inlets (secondary air, primary air, and fuel) the mass flow rates and temperatures have been prescribed according to the experimental data. A user function was used to impose the swirl motion of the primary air. The appropriate temperatures were prescribed for all wall boundaries. The values for wall emissivities, on

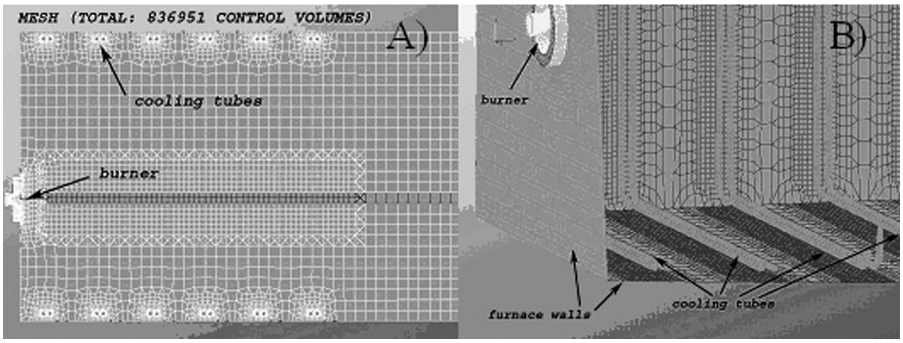

Figure 6. Unstructured computational mesh: (A) vertical cut along the axis (part; flame expecting region); (B) cooling tubes (side view; cut).

the other hand, were simply set to 0.7 and 0.5 for cooling tubes and all other walls, respectively. Adams and Smith [9] performed a sensitivity analysis for different values of wall and cooling tubes emissivities on a very similar geometry and found little influence of wall emissivities. This seems to be the case in examples with one dominant heat sink (cooling tubes), where different prescriptions of wall emissivity factor on surrounding walls do not play an important role.

Due to high computational demands of computational models used on relatively large computational mesh and due to finite computational power being available, the DTRM calculations were performed with 4 (1×4) and 8 (2×4) rays fired from each boundary cell face. A comparison of the predicted results for those different values of rays employed has been done. However, based on a previous experience on simpler cases [12] and other reports, such as [7, 8], better accuracy is expected if more rays are used in calculations. The calculation itself was steady state, with second-order spatial discretization schemes employed.

RESULTS

The simulated flow field characteristics are shown in Figure 7. Reversed flow regions occur at different locations and in an asymmetric pattern, emphasizing the three-dimensional nature of the flow. This behavior was expected due to the swirl motion imposed on the primary air inlet. Right after the burner, two recirculation zones can be observed as a consequence of swirl of the primary air, promoting efficient fuel/oxidizer mixing and contributing to improved combustion process. With the recognized weaknesses of k–ε turbulence modeling in cases where complex flow phenomena, such as swirl motion, streamline curvature effects, etc., can be found, as is the case here, the application of second-moment closures, or even improved k–ε versions, is expected to lead to more accurate flow field resolution.

The predicted axial temperature profiles at the centerline are shown in Figure 8, and they are compared to measured ones. Both predictions, with 4 rays and 8 rays used in the DTRM, show reasonable agreement with experimental data. The qualitative behavior follows closely the experimentally observed one, although the peak values are somewhat overpredicted. A better and more detailed combustion model,

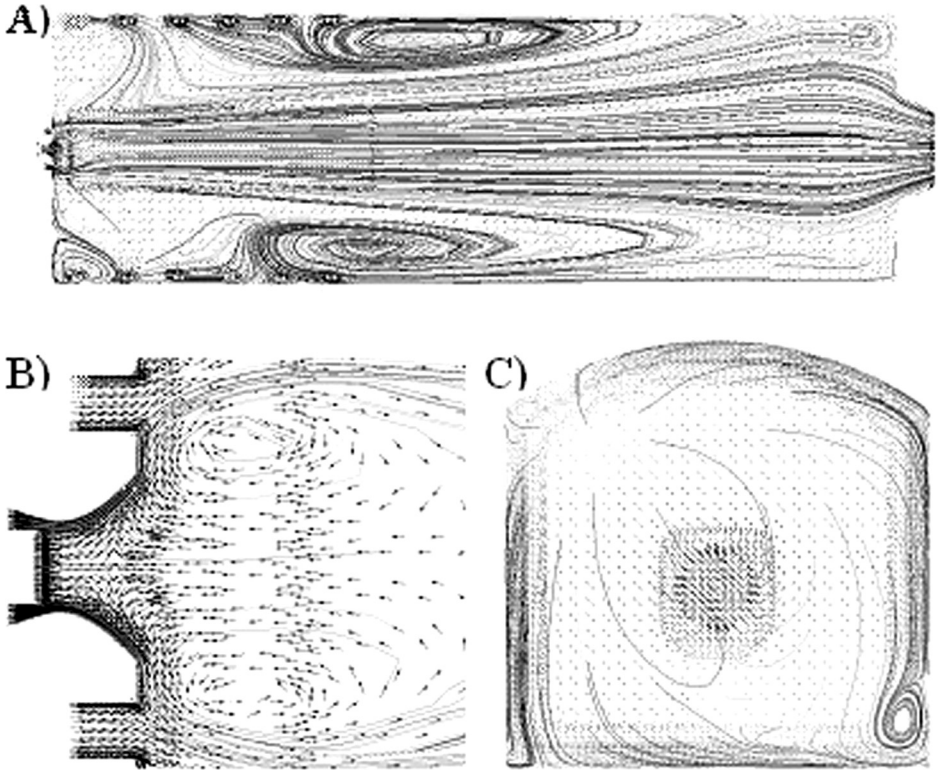

Figure 7. Predicted flow field: (A) streamlines and velocity vectors at horizontal plane (centerline position; view from above); (B) enlarged view on velocity vectors at horizontal plane near the burner (centerline position; view from above); (C) streamlines and velocity vectors on vertical plane offset 0.1 m from the burner (view in negative axis direction).

with spray effects included, would most likely bring an improvement in this respect. The difference between the two predictions with different numbers of rays used in the DTRM calculations is rather small, with slight improvement in peak temperature prediction in the case with more rays. A hypothetical test case, with radiation neglected, shows strong overpredicted temperatures, demonstrating once again the need for accurate radiative heat transfer simulation in large-scale configurations, like this one.

Table 1 shows the net heat flow rates on the domain boundaries. Four different predictions are presented, three of them with radiation and one hypothetical test case without radiation. According to the experimental data, the furnace load was around 1,800 kW, with the majority of the heat input coming from the sensible heat of air and fuel and the chemically bound energy of fuel. Slight differences in the net heat rates at mass flow inlets for different simulation cases are due to the net radiative heat exchange on those boundaries, which differs slightly among the cases. The inlet/outlet boundaries are considered as black surfaces when calculating radiative heat transfer on them. Table 1 shows the net heat flows obtained by the measurements as well.

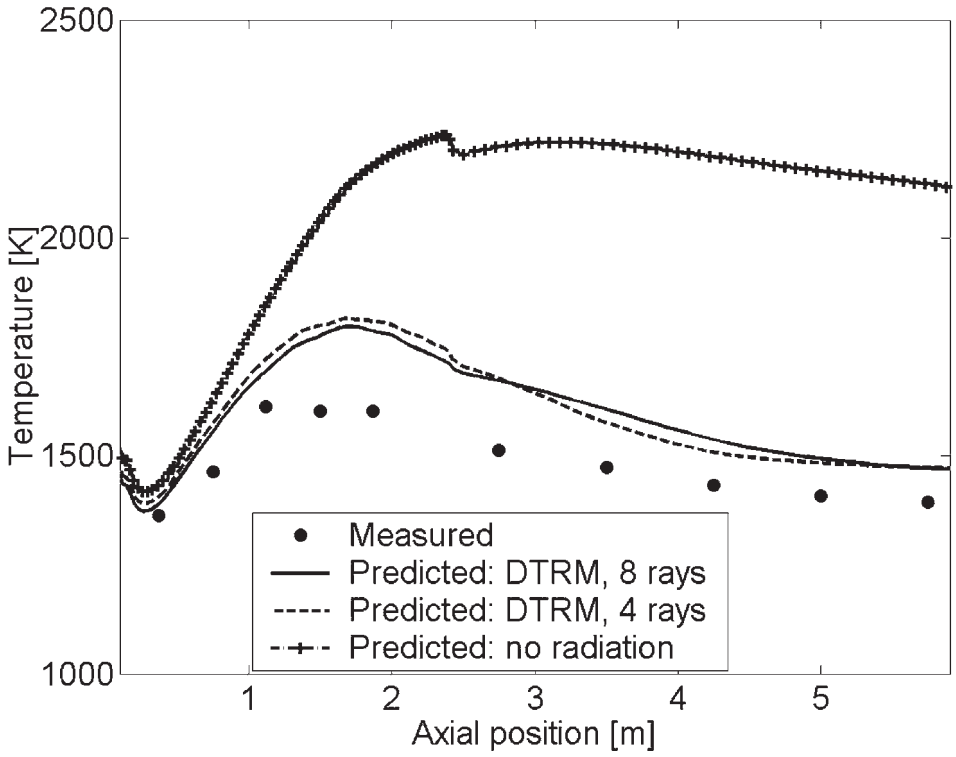

Figure 8. Measured and predicted axial temperature profiles at centerline position.

The predictions obtained with application of the conservative DTRM formulation, and for different numbers of rays, show good agreement with measured heat rates, and the overall heat misbalance is less than 2% of the net heat input. As expected, the cooling tubes represent the main wall heat sink in the domain, and the predicted values agree fairly well with measurements. The majority of the heat, however, leaves the furnace at the outlet as sensible heat of the flue gases. The heat losses on other wall boundaries (front, side, and rear wall), for which temperature

Table 1. Measured versus predicted heat balance at domain boundaries

		Predicted heat flow (kW)			
Boundary region	Measured heat flow (kW)	DTRM (4 rays)	DTRM (8 rays)	DTRM (8 rays; nonconservative)	No radiation
Mass flow inlets	1805.6	1802.2	1801.5	1798.6	1804.1
Outlet	−924.3	−972.1	−968.6	−952.5	−1516.1
Cooling tubes	−603.7	−631.7	−638.3	−601.9	−97.0
Other walls	−239.0	−230.5	−228.6	56.7	−222.6
Unaccounted	−38.6	−32.1	−34	300.9	−31.6
Unaccounted (%)	2.14	1.78	1.89	16.73	1.75

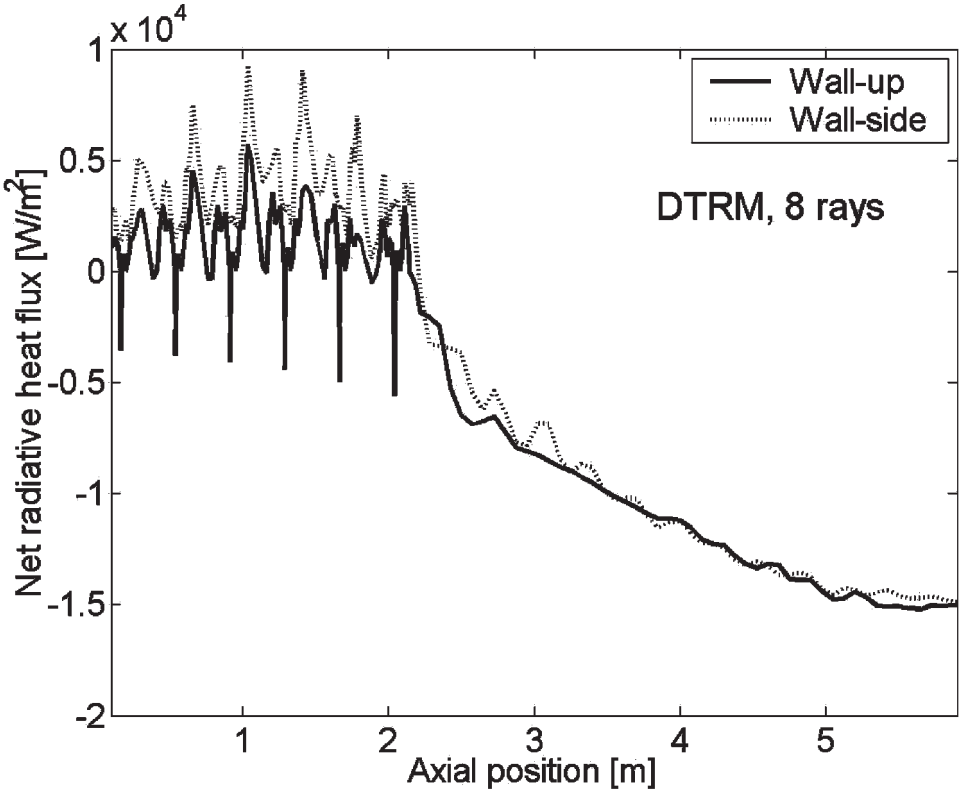

Figure 9. Predicted net radiative heat flux axial profiles at the walls.

measurements were mostly available, are in close agreement with experimental data. It is worthwhile to mention that approximately 8% of the overall heat on the cooling tubes is transferred by means of convection, while on other wall boundaries this fraction is much less. Similarly, no evidence of better accuracy of 8-ray DTRM over 4-ray DTRM can be deduced. However, the fact that more heat is transferred from the participating media to the cooling tubes (less heat transfer at the outlet) when 8 rays are used instead of 4 rays could indicate that the results are still sensitive to the number of rays used. Accordingly, more rays would certainly improve the temperature field by decreasing its overall value due to increased heat transfer to the cooling tubes.

Additional worthy information contained in Table 1 is the comparison of the conservative versus the original DTRM formulation. The predicted results obtained with the original DTRM formulation and 8 rays are shown. The problem of the nonconservative nature of this formulation, as addressed in [14], has emerged here as well. The energy misbalance in this prediction exceeds 16% of the total heat input, much worse than in the case with conservative formulation. While the heat flux on the cooling tubes is less sensitive to the different formulations employed, the heat fluxes at other wall boundaries showed different behavior. The small misbalance

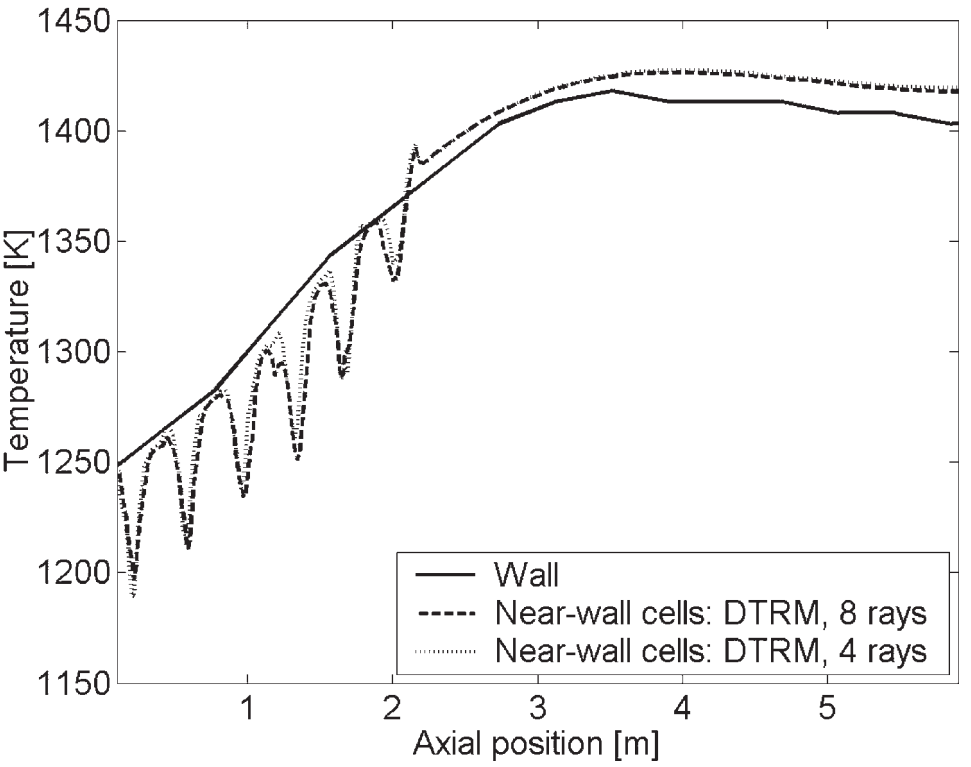

Figure 10. Axial temperature profiles in near-wall cells (wall side).

occurring in the conservative DTRM case is probably due to finite convergence achieved, just as in the hypothetical case without radiation.

Figure 9 shows the net radiative heat flux profiles at the walls positioned along the axis (side walls) and on two different locations—wall-up and wall side (see Figure 3). Due to insufficient experimental data, only predictions are shown. The shadowing effects on heat flux profiles are easy to identify, similarly as in [9, 10]. Dips in the heat flux profiles are the consequence of the cooling tubes positioned just in front of the wall, capturing some of the incoming radiation from the participating medium onto the wall. As can be seen in Figure 9, in the first part (approximately one-third) of the furnace length, where the cooling tubes are positioned along the wall, the heat flux on the side wall is due mainly to heat exchange with the surrounding cooling tubes, with negative peaks being responsible for radiative exchange with the participating medium. At other positions in the axial direction, the heat flux profiles are smoother.

Similar effects of the tubes can be observed on the axial temperature profile across the domain cells positioned just beside the side wall. Figure 10 shows this distribution, with imposed side-wall temperature serving as a guide. In this case, however, the temperature dips occur between the cooling tubes and surrounding wall, where relatively cold cooling tubes are responsible for low local temperature.

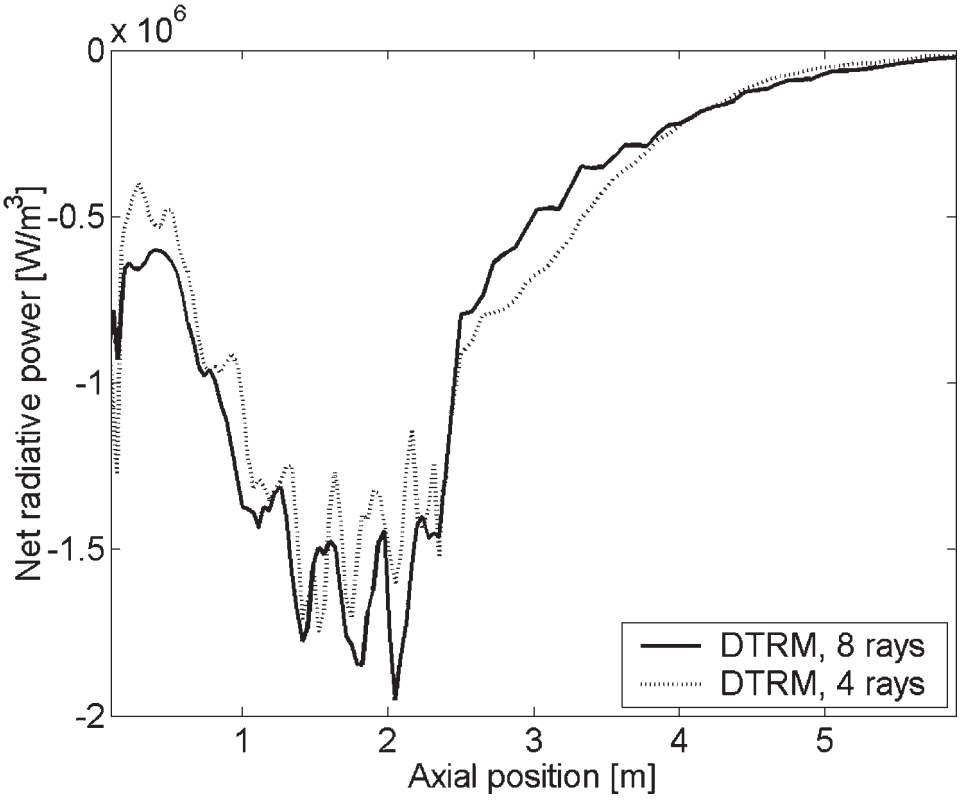

Figure 11. Predicted axial net radiative power profiles at centerline.

Figure 11 shows axial profiles of the net radiative power (source term intensity/cell volume) at the centerline for different numbers of rays used in DTRM calculations. As previously concluded, in the case when more rays are used, the heat transfer from the participating medium to the cooling tubes is increased, which is clearly reflected in the greater absolute value of net radiative power of the participating medium in the first part of the axial length. Six different local peaks in this profile, due to cooling tubes, can be seen also.

CONCLUSION

In this work it is shown that a conservative discrete transfer radiation method can be successfully applied for radiation prediction in CFD simulation of a furnace with complex geometry. The superiority of the conservative formulation over the original one is emphasized, especially when radiative heat fluxes on the domain boundaries are considered. The original formulation has been shown to be nonconservative, with conservative formulation being the preferred choice in complex geometries. Although only 8 rays have been used in the present work, the discrete

transfer method was able to capture directional shadowing effects on the net radiative heat flux distribution on the side walls. Besides being the major radiative heat sink in the domain, the cooling tubes, positioned just in front of the side walls, intercept the incoming radiation from the participating medium onto the side walls, causing the dips in the side-wall heat flux distribution. Cooling-tubes effects on net radiative power at the centerline have been observed as well. The difference between predicted results with 4 rays and 8 rays, is not substantial, but increased prediction accuracy is expected if more rays were used. The flow pattern, on the other hand, showed strong three-dimensional nature, emphasizing the need for complete domain modeling during simulation of similar problems with increased geometry complexity.

REFERENCES

1. T. R. Johnson, Application of the Zone Method of Analysis to the Calculation of Heat Transfer from Luminous Flames, Ph.D. thesis, University of Sheffield, 1971.
2. H. C. Hottel and A. F. Sarofim, *Radiative Transfer*, McGraw-Hill, New York, 1967.
3. J. R. Howell, Application of Monte Carlo to Heat Transfer Problems, *Adv. Heat Transfer*, vol. 5, pp. 1–54, 1968.
4. B. G. Carlson and K. D. Lathrop, Transport Theory—The Method of Discrete Ordinates, in H. Greenspan, C. N. Kelber, and D. Okrent, (eds.), *Computing Methods in Reactor Physics*, pp. 171–266, Gordon & Breach, New York, 1968.
5. W. A. Fiveland, Discrete-Ordinates Solutions of the Radiative Transport Equation for Rectangular Enclosures, *J. Heat Transfer*, vol. 106, pp. 699–706, 1984.
6. G. D. Raithby and E. H. Chui, A Finite Volume Method for Predicting Radiant Heat Transfer in Enclosures with Participating Media, *J. Heat Transfer*, vol. 112, pp. 415–423, 1990.
7. F. C. Lockwood and N. G. Shah, A New Radiation Solution for Incorporation in General Combustion Prediction Procedures, *Proc. 18th Int. Symp. on Combustion*, pp. 1405–1414, The Combustion Institute, Pittsburgh, PA, 1981.
8. M. G. Carvalho, T. Farias, and P. Fontes, Predicting Radiative Heat Transfer in Absorbing, Emitting and Scattering Media Using Discrete Transfer Method, *Fundam. Radiat. Heat Transfer*, vol. 160, pp. 17–26, 1991.
9. B. R. Adams and P. J. Smith, Three-Dimensional Discrete-Ordinates Modeling of Radiative Transfer in a Geometrically Complex Furnace, *Combustion Sci. Technol.*, vol. 88, pp. 293–308, 1993.
10. M. Y. Kim, S. W. Baek, and J. H. Park, Unstructured Finite-Volume Method for Radiative Heat Transfer in a Complex Two-Dimensional Geometry with Obstacles, *Numer. Heat Transfer B*, vol. 39, pp. 617–635, 2001.
11. AVL AST, SWIFT manual v3.1.1, AVL List GmbH, Graz, Austria, 2003.
12. M. Baburić, A. Raulot, and N. Duić, Implementation of Discrete Transfer Radiation Method into SWIFT CFD Code, in *Book of Abstracts, 11th Symp. of Thermal Engineers from Serbia and Montenegro*, Energy, Energy Efficient and Ecologically Acceptable Processes in Thermal, Chemical and Process Engineering, Zlatibor, Serbia and Montenegro, pp. 62–63, 2003.
13. M. Baburić, N. Duić, A. Raulot, R. Tatschl, and B. Wiesler, Accurate Discrete Transfer Radiation Modelling in Industrial Furnaces—A Validation Study, *Proc. Conf. on Modelling Fluid Flow*, Budapest, Department of Fluid Mechanics, Budapest University of Technology and Economics, pp. 262–268, 2003.
14. P. J. Coelho and M. G. Carvalho, A Conservative Formulation of Discrete Transfer Method, *J. Heat Transfer*, vol. 119, pp. 118–128, 1997.

15. AVL AST, CFD Workflow Manager manual v1.1.1, AVL List GmbH, Graz, Austria, 2003.
16. M. Baburić, Ž. Bogdan, and N. Duić, A New Approach to CFD Research: Combining AVL's Fire Code with User Combustion Model, *Proc. 24th Int. Conf. Information Technology Interfaces ITI 2002*, June 24–27, 2002.
17. T. F. Smith, Z. F. Shen, and J. N. Friedman, Evaluation of Coefficients for the Weighted Sum of Gray Gases Model, *J. Heat Transfer*, vol. 104, pp. 602–608, 1982.